energies

MDPI

Article

A Eutectic Mixture of Calcium Chloride Hexahydrate and Bischofite with Promising Performance for Thermochemical Energy Storage

Bryan Li [1], Louise Buisson [2], Ruby-Jean Clark [1], Svetlana Ushak [3] and Mohammed Farid [1,*]

[1] Department of Chemical and Materials Engineering, The University of Auckland, Auckland 1010, New Zealand; bryan.li@auckland.ac.nz (B.L.); ruby-jean.clark@phasefoam.com (R.-J.C.)
[2] EPF School of Engineering, 94230 Cachan, France; louise.buisson@epfedu.fr
[3] Center for Advanced Study of Lithium and Industrial Minerals (CELiMIN) and Departamento de Ingeniería Química y Procesos de Minerales, Universidad de Antofagasta, Campus Coloso, Avenida Universidad de Antofagasta, Antofagasta 02800, Chile; svetlana.ushak@uantof.cl
* Correspondence: m.farid@auckland.ac.nz

Abstract: Thermochemical energy storage using salt hydrates is a promising method for the efficient use of energy. In this study, three host matrices, expanded vermiculite, expanded clay, and expanded natural graphite were impregnated with a eutectic mixture of $CaCl_2 \cdot 6H_2O$ and bischofite ($MgCl_2 \cdot 6H_2O$). These composites were subjected to various humidity conditions (30–70% relative humidity) at 20 °C over an extended hydration period to investigate their cyclability. It was shown that only expanded natural graphite could contain the deliquescent salt at high humidity over 50 cycles. Hence, the expanded natural graphite composites containing either $CaCl_2 \cdot 6H_2O$ or $CaCl_2 \cdot 6H_2O$/bischofite eutectic mixture were placed in a lab-scale open packed bed reactor, providing energy densities of 150 and 120 kWh/m^3 over 20 h, respectively. The eutectic composite showed slightly lower temperature lift, water uptake rate, and power output but at reduced cost. Using the eutectic mixture also decreased the composite's dehydration temperature at which the maximum mass loss rate occurred around 16.2 °C to 62.3 °C, allowing recharge using less energy-intensive heating methods. The cost of storing 1 kWh of energy with expanded natural graphite composites is only USD 0.08 due to its stability. This research leveraging cost-effective composites with enhanced stability, reaction kinetics, and high thermal energy storage capabilities benefits renewable energy, power generation, and the building construction research communities and industries by providing a competitive alternative to sensible heat storage technologies.

Keywords: calcium chloride hexahydrate; bischofite (magnesium chloride hexahydrate); eutectic; expanded natural graphite; expanded vermiculite; expanded clay; thermochemical energy storage

Citation: Li, B.; Buisson, L.; Clark, R.-J.; Ushak, S.; Farid, M. A Eutectic Mixture of Calcium Chloride Hexahydrate and Bischofite with Promising Performance for Thermochemical Energy Storage. *Energies* **2024**, *17*, 578. https://doi.org/10.3390/en17030578

Academic Editor: Francesco Fornarelli

Received: 23 December 2023
Revised: 15 January 2024
Accepted: 17 January 2024
Published: 25 January 2024

1. Introduction

Thermal energy storage (TES) can increase the efficiency and flexibility of renewable energy systems [1,2]. TES can be classified into three categories: sensible heat storage (SHS), latent heat storage (LHS), and thermochemical energy storage (TCES). Compared to commercially available SHS and LHS technologies, TCES is the most promising, as it has several positive elements, such as high energy storage density, long storage period, and negligible system heat losses [2]. Salt hydrates have been widely employed in TCES, where heat is recovered through an exothermic reaction with humid air, one of the most abundant resources on earth [3,4]. A key advantage of this reaction is its reversibility, whereby energy can be stored via dehydration using hot, dry air, enabling reuse when needed [5].

There are practical problems in the application of salt hydrates in TCES, including corrosivity, low thermal conductivity, slow kinetics, and material deterioration by agglomeration or melting [6–8]. A widely accepted solution to these challenges is the use of a porous

host matrix for implementation at scale [2]. Previous studies have examined the efficacy of a myriad of salts for application in TCES, including $SrCl_2 \cdot 6H_2O$ [7,9], $SrBr_2 \cdot 6H_2O$ [10–12], $MgCl_2 \cdot 6H_2O$ [13,14], $CaCl_2 \cdot 6H_2O$ [6,15,16], $(NH_4)_2Zn(SO_4)_2 \cdot 6H_2O$ [17], $MgSO_4$ [13,18], $LiOH \cdot H_2O$ [19,20], and K_2CO_3 [21]. Many methods were used to impregnate the aforementioned salts into porous matrices mostly via molten salt hydrate impregnation [6,15] and aqueous solution impregnation [6,15,16,22] at standard pressure and elevated temperature. The host matrices have included synthetic polymers [23], expanded natural graphite (ENG) [12,16,18–21,23], expanded vermiculite (EV) [16,24,25], expanded clay (EC) [7], and cement [9,26]. Their performance has been investigated under a range of hydration conditions, with temperatures of 13–35 °C and relative humidity (RH) from 30% to 90%. However, with extended hydration time and cycling above deliquescence conditions, the salt solution was found to leak out of the matrix [27]. This is extremely detrimental, as the extractable energy will decrease over time and the leakage can cause fast and severe corrosion, requiring replacement of the composites and reactor parts.

Much of the existing literature on TCES using salt-impregnated matrices has overlooked the long-term performance under practical scale or challenging hydration conditions [4,6,15,16,18]. For example, studies on salt-impregnated ENG have had little emphasis on success with practical cyclability beyond the scale of TGA/DSC. Gaeini et al. impregnated ENG with 73 wt. % $CaCl_2$ using solution impregnation, which was increased to 87 wt. % with successive impregnation [16]. This corresponds to >400 kWh/m^3 theoretical energy density; however, leakage occurred within 10 TGA/DSC cycles of hydration at 20 °C, 86% RH, and dehydration at 80–150 °C. As a result, only 167 kWh/m^3, or 40% of the theoretical energy density was accomplished experimentally. To prevent deliquescence, Druske et al. and Korhammer et al. impregnated ENG with $CaCl_2 \cdot 6H_2O$ and KCl through solution and molten impregnation, reporting an energy density of 162 kWh/m^3. However, this was also tested with small samples using TGA/DSC, which provided no conclusions on stability over cycles or the performance of larger sized particles where mass transfer is impeded [15]. Both studies have a very limited focus on practical performance in a real-life scenario. Similar work and conclusions were drawn from ENG/$MgCl_2$ composites, where a maximum of 60 cycles were completed in TGA/DSC, showing a 14.2% reduction in storage density [13,14].

Furthermore, only a few authors have investigated the performance of composites in a lab-scale open reactor. Strontium chloride impregnated in EC (40 wt. %) [7], pumice (14 wt. %) [7], and cement (50 wt. %) [9] achieved 29 kWh/m^3, 7.3 kWh/m^3, and 136 kWh/m^3, respectively. The cement and pumice composites showed stability over 5 and 10 cycles, respectively, while EC failed from the second cycle due to the challenging hydration conditions (20 °C, 80% RH). Similar work has been carried out with calcium chloride impregnated composites, including aerated porous concrete (43 wt. %) [26] and vermiculite (56 wt. %) [26], obtaining energy densities of 187 kWh/m^3 and 112 kWh/m^3, respectively, but only over three cycles.

$CaCl_2 \cdot 6H_2O$ and $MgCl_2 \cdot 6H_2O$ are both hygroscopic, offering a promising energy densities of 601 kWh/m^3 and 547 kWh/m^3, respectively [28]. Due to the increasing importance of byproduct and waste utilization for both environmental and economic benefits, it is of interest to substitute $MgCl_2 \cdot 6H_2O$ with bischofite, the main byproduct of potassium and lithium extraction in Salar de Atacama (north of Chile), Israel, and the Netherlands [29,30]. It contains more than 95% $MgCl_2 \cdot 6H_2O$ and shows very similar physical and thermochemical characteristics to synthetic $MgCl_2 \cdot 6H_2O$ (approximately 101 °C melting point and 520 kWh/m^3). It has already been investigated as a phase change material [29,30]. Bischofite is more than three times cheaper than synthetic $MgCl_2 \cdot 6H_2O$ [29], at USD 0.16 per kg, due to its natural occurrence in salt deposits, requiring less processing and energy input, as well as it being a waste byproduct from lithium and potassium extraction. The simpler extraction process, lower water content, and geographical factors contribute to the cost-effectiveness of bischofite compared to the hexahydrate form of magnesium chloride and calcium chloride. Replacing synthetic $MgCl_2 \cdot 6H_2O$ with bischofite in TCES can greatly

reduce the composite cost, offering significant potential in affordable TCES applications. Contrary to the low melting point of $CaCl_2 \cdot 6H_2O$ at around 30 °C, the melting point of $MgCl_2 \cdot 6H_2O$ and bischofite are significantly higher, at 123 °C [31] and 101 °C, respectively. Furthermore, the melting point of $MgCl_2 \cdot 6H_2O$ is higher than the dehydration temperature (118 °C [29]), making it infeasible to impregnate as molten $MgCl_2 \cdot 6H_2O$. As a result, successive impregnation with a saturated solution at higher temperatures is necessary to impregnate the desired amount of salt into the matrix. Fortunately, studies have found that mixtures of $CaCl_2 \cdot 6H_2O$ (75 wt. %)/$MgCl_2 \cdot 6H_2O$ and $CaCl_2 \cdot 6H_2O$ (75 wt. %)/bischofite have a low eutectic melting temperature of 21 °C, making the impregnation of bischofite more economical and avoiding high-temperature degradation [32].

To enable practical and scalable TCES technologies, the present study will evaluate and compare the composites' energy storage capacity, cyclability, and cost-effectiveness at both the single-particle and multi-particle packed bed levels, with high humidity and long hydration periods. The most important novelty is the use of the bischofite (a waste byproduct) in a stable composite with good reaction kinetics and high thermal energy storage capabilities, and at a low cost. Further, bischofite has a high melting point which makes its impregnation difficult. In this study, $CaCl_2 \cdot 6H_2O$ was used with bischofite, providing a eutectic mixture having a low melting temperature needed for impregnation. This is also the first time in the literature where the suitability of $CaCl_2 \cdot 6H_2O$/bischofite ENG, EV, EC composites have been investigated for TCES application. The stability of the composites is tested first in the humidity chamber over 50 cycles. Subsequently, the most stable composites are put in a packed bed reactor, where the volumetric thermal energy density, temperature lift, and overall performance are evaluated with varying inlet air flow rate and humidity. By doing so, we aim to provide insights that can enhance the performance, viability, and competitiveness of salt-in-matrix TCES technologies in real-world applications.

2. Materials and Methods

2.1. Composite Material Development

Synthetic $CaCl_2 \cdot 6H_2O$ (>97%) was purchased from Sigma-Aldrich (Auckland, New Zealand). Bischofite obtained from the brines concentration process and commercialized by Salmag (Antofagasta, Chile) was mixed with molten $CaCl_2 \cdot 6H_2O$ (75 wt. %) to create a eutectic mixture.

EV and EC were purchased locally from New Zealand, while ENG was obtained from NETenergy (Chicago, IL, USA). The host materials' physical characteristics were measured in the laboratory and costs were obtained from the manufacturers, as specified in Table 1.

Table 1. Host matrix material characteristics and cost.

Name	Dimensions	Density (kg/m^3)	Cost (USD/kg)
ENG	1 × 1 × 1 cm	190	2
EV	1 × 1 × 1 mm	100	0.3
EC	7 mm diameter	1000	0.13

Particles of each host matrix were submerged in molten salt hydrate in a closed container overnight in an oven at 40 °C. The composite material was then filtered with a mesh and dehydrated. Note that despite the fact that $CaCl_2 \cdot 6H_2O$ and the eutectic mixture melt at 30 °C and 21 °C, respectively, a temperature higher than the melting point was used to ease impregnation and ensure that the salt hydrate does not solidify during the post-impregnation separation of salt hydrate and composite.

2.2. Humidity Chamber Analysis

Single composite particles were placed in the Vötschtechnik humidity chamber at relative humidity ranging from 30% to 70% and 20 °C for over 20 h to investigate the effect of humidity on their cyclability and reaction rate. The particles were dehydrated in an oven at 130 °C until the composite materials reached a constant weight, where $CaCl_2$ and $MgCl_2 \cdot 2H_2O$ were formed [33].

2.3. STA Analysis

A thermal analyzer (STA 449 F5 Jupiter, NETZSCH, Selb, Germany) was used to investigate the dehydration behavior and endothermic effect of selected composites after hydration. A known mass of the sample (approximately 15 mg) was placed in an alumina crucible and subjected to a constant heating rate of 5 °C/min from room temperature to 200 °C whilst the chamber was continuously fed with argon as inert gas at 50 mL/min.

2.4. Reactor System Description and Experimental Setup

To further examine the performance of composites, a lab-scale packed bed reactor (Figure 1) was used and made from a 298 mm long cylindrical glass tube with 22 mm radius and 5 mm wall thickness. The reactor was insulated with 12 mm thick neoprene. Compressed air was fed into the FC Series™ humidifier (Perma Pure, NJ, USA) at the desired temperature and flow rate to humidify the air. The reactor was operated at atmospheric pressure. Data were recorded by two temperature–humidity sensors (HygroClip2 (Rotronic AG, Bassersdorf, Switzerland) screw-in probe with a temperature accuracy of ±0.1 °C and relative humidity accuracy of ±0.8% RH) placed at the inlet and outlet of the reactor and temperature sensors (Type K thermocouple (RS Components, London, UK) with an accuracy of ±0.4%) at the inlet, middle, and top of the reactor. The data were digitized using a data logger and recorded on a computer. To investigate the effect of inlet air flow rate and humidity, four conditions—20 L/min at 50%, 60%, and 70% RH, as well as 30 L/min at 70% RH—were used, while the inlet temperature was kept constant at 20 °C. These hydration/dehydration experiments were carried out in duplicate, totaling 8 cycles for each composite.

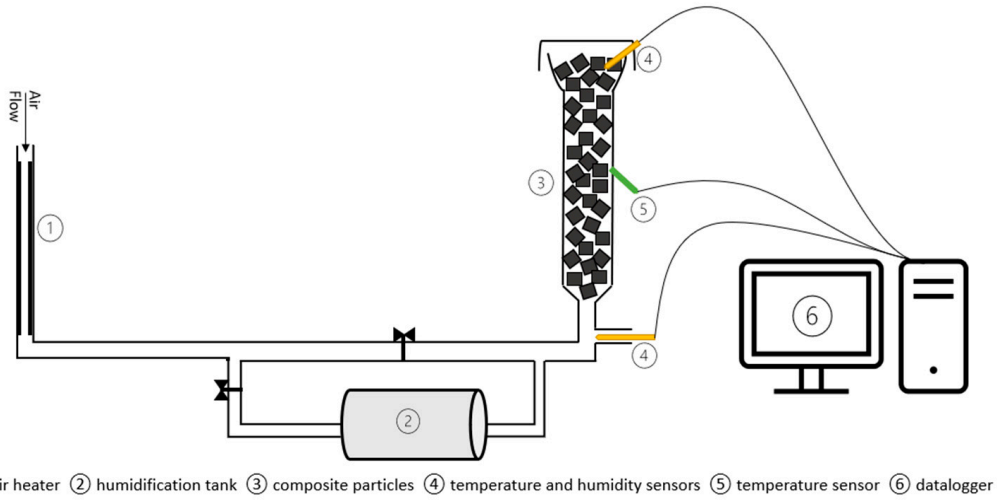

Figure 1. Packed bed hydration reactor schematic.

Following the conclusion of hydration reactions, the composite particles were dehydrated in the oven at 130 °C. When the mass of the particles was constant, they were quickly transferred to a container and were allowed to cool at ambient temperature. The container was tightly sealed to reduce hydration during cooling.

3. Results and Discussion

3.1. Composite Material Development

3.1.1. Salt Selection and Evaluation

Important considerations in the selection of salts for TCES included hydration/dehydration kinetics, energy density, ease of impregnation, and price. To generate substantial power from a hydration reaction, the salts used for this study were hygroscopic in nature so that high water uptake rate could be obtained. High water uptake directly relates to an increase in power output and overall volumetric energy density. Chlorides have been used extensively for TCES. Due to the strength and nature of the bonds between the salt and water molecules within the hydrate crystal lattice, it has been reported that $CaCl_2 \cdot 6H_2O$ can lose up to 6 moles of water below 100 °C [33], while $MgCl_2 \cdot 6H_2O$ can lose up to 4 moles of water below 130 °C, obtaining 601 kWh/m^3 and 547 kWh/m^3, respectively (Table 2) [28,29]. Lower dehydration temperature is preferable, as this lowers the quality of energy required to charge the material and makes recharging with solar energy possible. Furthermore, it improves the thermal efficiency of the system. Replacing pure $CaCl_2 \cdot 6H_2O$ with the synthetic $CaCl_2 \cdot 6H_2O/MgCl_2 \cdot 6H_2O$ eutectic mixture came at the cost of 2.2% less energy density, while their prices are similar (Table 2). In comparison, replacing pure $CaCl_2 \cdot 6H_2O$ with the bischofite eutectic mixture reduced the energy density by 3.6%, while lowering the cost by approximately 18%, as calculated based on mass fraction. Therefore, this study will only use the bischofite eutectic mixture to compare with pure $CaCl_2 \cdot 6H_2O$ for further investigation. Using the eutectic mixture made molten impregnation containing $MgCl_2 \cdot 6H_2O$ possible, as the melting point was reduced by approximately 100 °C. It could also offer less energy demand during composite preparation compared to pure $CaCl_2 \cdot 6H_2O$ due to the decreased melting point.

Table 2. Energy storage density at a dehydration temperature of 130 °C and salt hydrate cost.

Name	Energy Density (kWh/m^3)	Cost (USD/kg)
$CaCl_2 \cdot 6H_2O$	601	0.6 [34]
$MgCl_2 \cdot 6H_2O$	547	0.52 [29]
Bischofite	520	0.16 [29]
Eutectic mixture (25% of $MgCl_2 \cdot 6H_2O$)	588	0.58
Eutectic mixture (25% of bischofite)	580	0.49

3.1.2. Host Matrix Selection and Evaluation

Three matrices were considered: expanded natural graphite, expanded clay, and expanded vermiculite. All three are commercially available and are inexpensive. Each of these materials has unique properties and advantages and they can all be used for TCES by absorbing and releasing heat through reversible chemical reactions. Therefore, the choice of material will depend on the specific application, such as the energy storage capacity and operating conditions. In terms of customizing shapes for thermochemical energy storage, expanded clay presents challenges due to its relatively rigid nature, limiting intricate designs. In contrast, expanded vermiculite offers greater flexibility, allowing for more adaptable shapes and configurations. Expanded natural graphite falls in between, offering moderate customization possibilities, balancing formability with structural integrity for tailored energy storage solutions. While expanded clay offers excellent thermal stability and mechanical strength, expanded vermiculite provides enhanced heat transfer properties and lightweight characteristics; on the other hand, expanded natural graphite excels in its high thermal conductivity, making it a promising choice for efficient and rapid energy storage applications.

To evaluate the impregnation performance and compare the composites, the mass fraction of salt hydrate in the impregnated composite (Equation (1)) and that of anhydrous salt in the dehydrated composite (Equation (2)), as well as the composite density (Equation (3)) were calculated first.

$$x_{salt\ hydrate} = \frac{m_1 - m_0}{m_1} \tag{1}$$

where m_1 is mass of the composite after molten salt impregnation and m_0 is mass of the host matrix.

$$x_{salt} = \frac{(m_1 - m_0) \times \frac{M_{salt}}{M_{salt\ hydrate}}}{m_0 + (m_1 - m_0) \times \frac{M_{salt}}{M_{salt\ hydrate}}} \tag{2}$$

where M_{salt} is the molecular weight of the anhydrous salt and $M_{salt\ hydrate}$ is the molecular weight of salt hydrate.

$$\rho_{composite} = \rho_{matrix} \times \frac{m_1}{m_0} \tag{3}$$

where ρ_{matrix} is the density of the non-impregnated matrix.

The reactor cost is proportional to reactor volume and the composite densities varied significantly depending on the host matrix. Therefore, to meaningfully compare the composites, the volumetric energy density was calculated with Equation (4). The resultant volumetric energy density is different to the commonly reported salt volumetric energy density, as this calculation accounts for the void in the composites.

$$E_V = \frac{m_1 - m_0}{m_0} \times \rho_{matrix} \times \frac{M_{salt}}{M_{salt\ hydrate}} \times \Delta h \tag{4}$$

where Δh is the energy released from the hydration reaction. Unit conversions were carried out to express E_V in kWh/m^3 to compare with other studies.

The impregnation performance is summarized in Table 3. As shown in the table, the composite density of EC is significantly higher than ENG and EV, with ENG being the lowest. From the results of molten impregnation, the mass intake of salt is inversely proportional to the density of the composite, with 85% of hydrated salt in EV compared with only 32% in EC. It was also found that the impregnation performance was similar for the same matrix regardless of the composition of the molten salt. This aligns with the theory that the diffusion of molten salt into the matrix is dependent on the liquid viscosity, matrix porosity and density, temperature, and duration of soaking. Since all the parameters were similar during the impregnation of the same matrix, it was expected that the impregnation performance would also be similar.

Table 3. Composite characteristics.

Composite Host Matrix Material	Hydrated Composite Density (kg/m^3)	Wt. % of Hydrated Salt	Anhydrous Composite Density (kg/m^3)	Wt. % of Anhydrous Salt	Energy Density Upon Forming X·6H$_2$O (kWh/m^3)	
					$CaCl_2$	Eutectic
ENG	570	67	380	50	180	163
EV	670	85	400	75	266	239
EC	1470	32	1240	19	221	199

The high density of EC means its volumetric salt intake is higher than ENG. Due to the absorbent nature of EV, both its mass and volumetric salt intake are the highest. Comparatively, the theoretical energy density of ENG is the lowest, as it has neither the highest density nor porosity. However, this does not mean that ENG is a poor candidate. This is because the theoretical energy density does not take the overhydration of salt (deliquescence) into account, which can commonly cause leakage, resulting in less salt in

the matrix, corresponding to less extractable energy. The composite's ability to contain deliquescence is especially important when it contains highly hygroscopic salts such as $CaCl_2$, which easily overhydrates at above 20 °C, 30% RH [25,35]. In addition, since $CaCl_2 \cdot 6H_2O$ and the eutectic mixture have a very low melting point, it is possible that in practical applications, the ambient temperature will exceed the melting point. The result is that the salt hydrates within the composite are molten and could be prone to leakage. Furthermore, it is important to consider whether the salt can be fully hydrated and dehydrated due to water vapor pathways being open in the composite; there is overloading of salt blocking pores for vapor pathways and the composites can be cycled without decrease in mechanical properties.

The composite and energy cost of each composite are summarized in Table 4. The composite cost per mass, volume, and energy is the highest for ENG composites due to the high cost of the matrix. For the same weight, the cost of ENG composites is 120% more than EV and 300% more than EC. To fill a reactor, the cost of EV is between approximately USD 310 and USD 375 per m^3, around 16% cheaper than EC, while that of ENG is over USD 570 per m^3. The price of the energy that can be stored and extracted is similar between salts using the same matrix. The energy cost is the lowest for EV at around USD 1.3 per kWh, which is 28% cheaper than EC and 66% cheaper than ENG. However, this energy price comparison assumes that the composites can be used for the same number of cycles, i.e., no leakage or any deterioration, and all the theoretical energy can be utilized. To meaningfully compare the energy prices offered by the composites, the cyclability must be tested first under a range of hydration conditions and for extended periods of time, followed by tests in an open PBR if the cyclability is satisfactory.

Table 4. Composite cost.

Composite Type	Composite Cost (USD/kg)		Composite Cost (USD/m^3)		Energy Cost (USD/kWh)	
	$CaCl_2$	Eutectic	$CaCl_2$	Eutectic	$CaCl_2$	Eutectic
ENG	1.1	1.0	627	570	3.5	3.5
EV	0.56	0.46	375	308	1.4	1.3
EC	0.28	0.25	412	368	1.9	1.8

3.2. Hydration Characteristics of Single Particles

3.2.1. Effect of Humidity on Cyclability

The composites are defined to be unstable by three factors: leakage of impregnated material, changes in mechanical properties that can result in premature failure, and a change in water uptake decreasing achievable energy density over cycles. Leakage and changes in mechanical properties are significant when the salt in the composite undergoes deliquescence. Therefore, it is important to apply conditions to achieve the maximum experimental energy density and to understand the composites' limits. This was carried out in the humidity chamber at 30% to 70% RH and 20 °C.

To determine if there is salt loss due to deliquescence or salt melting at elevated temperatures during hydration and dehydration, the dehydrated composite mass was recorded for every cycle. The salt mass was calculated as the difference between the recorded mass and the original matrix mass, and the ratio of salt mass to original matrix mass is plotted in Figure 2. The salt underwent deliquescence and leaked for all composites initially, which decreased as cycling progressed at 30% RH. Both ENG/$CaCl_2$ and ENG/eutectic composites were initially cycled over 10 times and appeared stable under 30%, 50%, and 70% RH at 20 °C. Under 30% RH and 20 °C, the water uptake by EC consistently corresponded to energy density just below the full theoretical energy density at 160 kWh/m^3 without noticeable mechanical deterioration. This indicates that the salt in the EC was not fully hydrated for the same duration that ENG and EV were, most likely due to poor diffusion. Despite

the high volumetric salt intake of EV and EC, cycling results show that under 50% RH, both were unable to retain deliquescence. This was due to faster hydration kinetics influenced by higher water vapor pressure, leading to more deliquescence in the matrix over the same hydration period and causing leakage. The salt continued to leak out throughout cycles until little was left, resulting in low achievable energy density. This result suggests that EV and EC are not suitable to operate in deliquescence conditions, especially over extended periods of time. This also means that the EV and EC composites used for this study may not be practical in certain real-life circumstances, such as in building ventilation where air drawn from the atmosphere can have high humidity over extended periods.

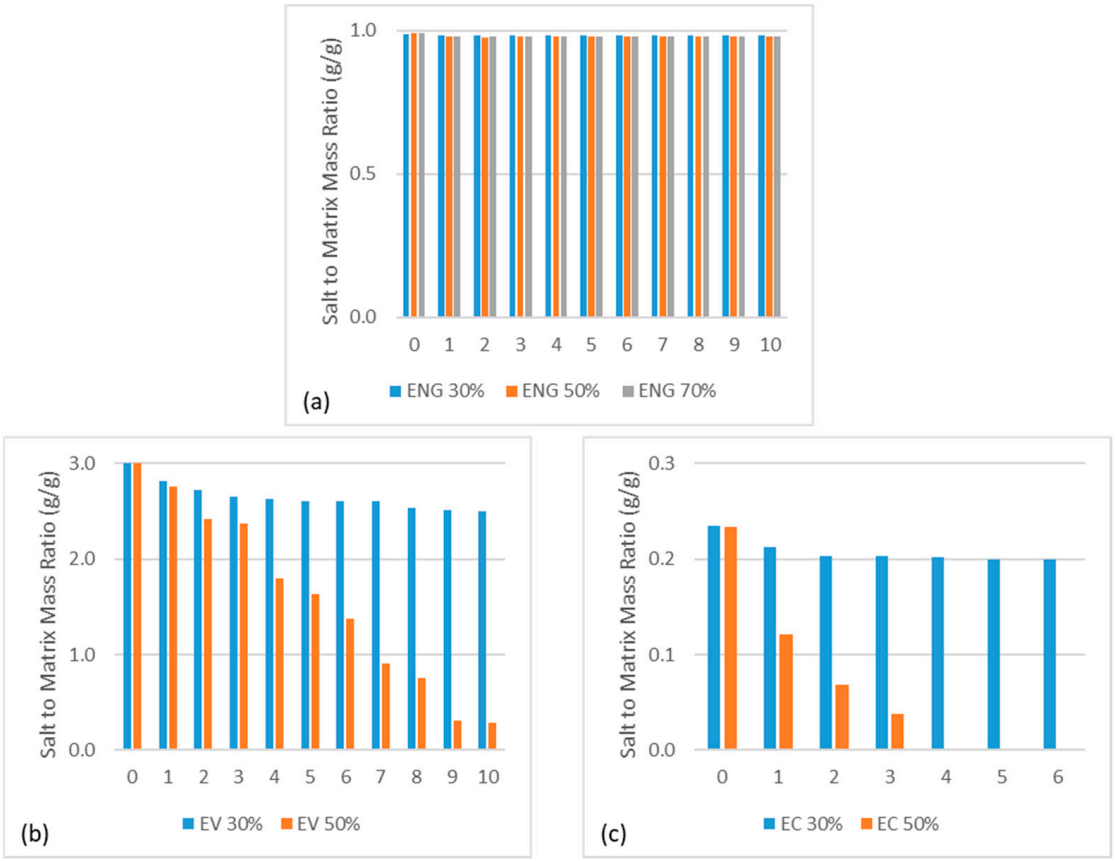

Figure 2. Salt to original matrix mass ratio over hydration/dehydration cycles at 20 °C and varying humidity of (**a**) ENG, (**b**) EV, and (**c**) EC $CaCl_2$ composites.

So far, ENG appears to be the most suitable composite due to its cyclability despite its high material cost and low volumetric salt intake. To further test this composite, more cycles were performed and the specific water uptake was calculated for each cycle (Figure 3). In total, 45 cycles and 30 cycles were completed for ENG $CaCl_2$ and eutectic composites, respectively, at 20 °C and 50% RH (Figure 3a), where the water uptake of both ENG composites was consistent. The water uptake of ENG/$CaCl_2$ composite was around 1.8–2.0 g water/g salt, approximately 50% higher than what is required to form the hexahydrate, which indicates that the salt is deliquescent. It was also observed that the eutectic mixture had 10% less performance due to the incomplete dehydration at 130 °C. Hydration in more extreme conditions was also carried out under 20 °C and 70% RH (Figure 3b), where both composites appeared stable over 10 cycles with higher water uptake.

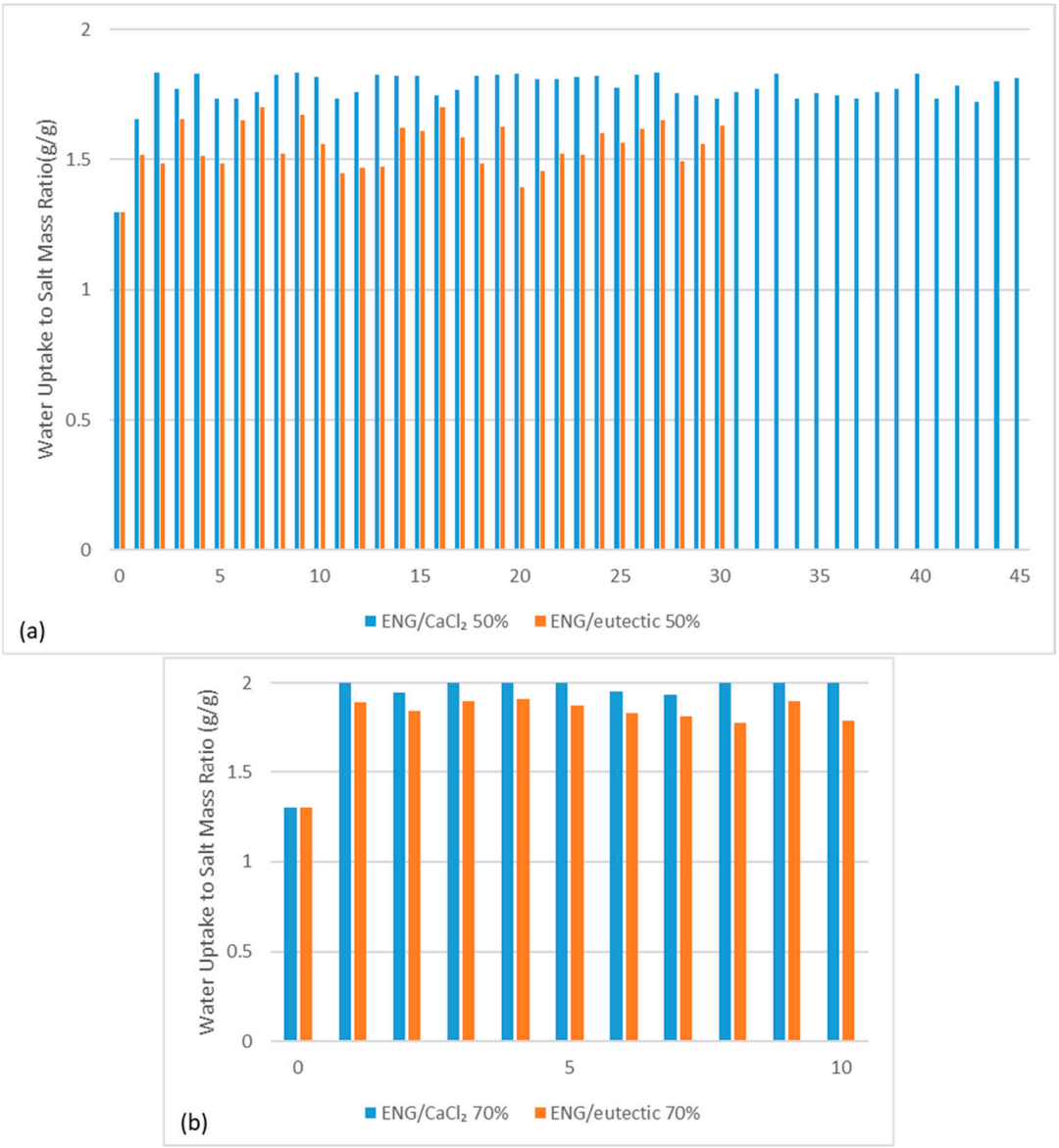

Figure 3. Hydration cycling of ENG $CaCl_2$ and eutectic composites at 20 °C and (**a**) 50% RH and (**b**) 70% RH.

3.2.2. Rate of Reaction of Single ENG Particles

Following the successful cycling of ENG composites, rate of reaction studies were carried out to evaluate the rate of water uptake of single particles, which is important for scale-up implementation (Figure 4). At 70% RH, the salt in ENG could uptake 6 moles of water in 3.5 h, whereas at 50% RH, more than 5 h was required. This is because the partial pressure of water vapor increases the rate of reaction [33]. The water uptake rate of ENG/eutectic was slower than ENG/$CaCl_2$ for all conditions tested due to the fact that $MgCl_2$ is less hygroscopic than $CaCl_2$. From the results above, ENG is the best candidate for hosting highly hygroscopic salts. It has shown to be stable over 50 cycles even with deliquescence and can achieve high energy density, with a reasonable water uptake rate.

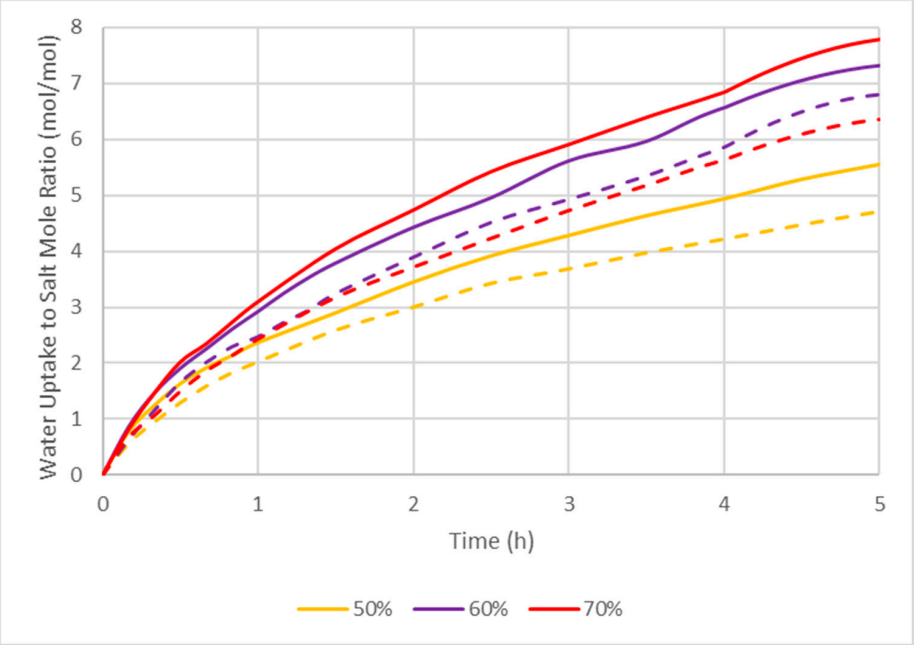

Figure 4. Mole-based water uptake behavior of ENG $CaCl_2$ (solid lines) and eutectic (dotted lines) composites at 20 °C and 50%, 60%, and 70% RH.

3.2.3. STA Analysis

Upon hydration at 70% RH, both ENG composites were then analyzed with STA as shown in Figure 5. The water mass loss for ENG/$CaCl_2$ is at 45.7%, which is higher than the 37.4% achieved from ENG/eutectic. This aligns with the water uptake difference observed during single ENG particle hydration studies (Section 3.2.2). The maximum dehydration rate also occurred at different temperatures, which is 62.3 °C for the ENG/eutectic composite, which is 16.2 °C lower than the ENG/$CaCl_2$ composite. The mass loss of ENG/eutectic was also greater than ENG/$CaCl_2$ below 80 °C. This suggests that the eutectic composite can be recharged at a lower temperature, which is advantageous, allowing for the use of less energy-intensive heating methods, such as solar energy or low-temperature waste heat, to trigger the recharge.

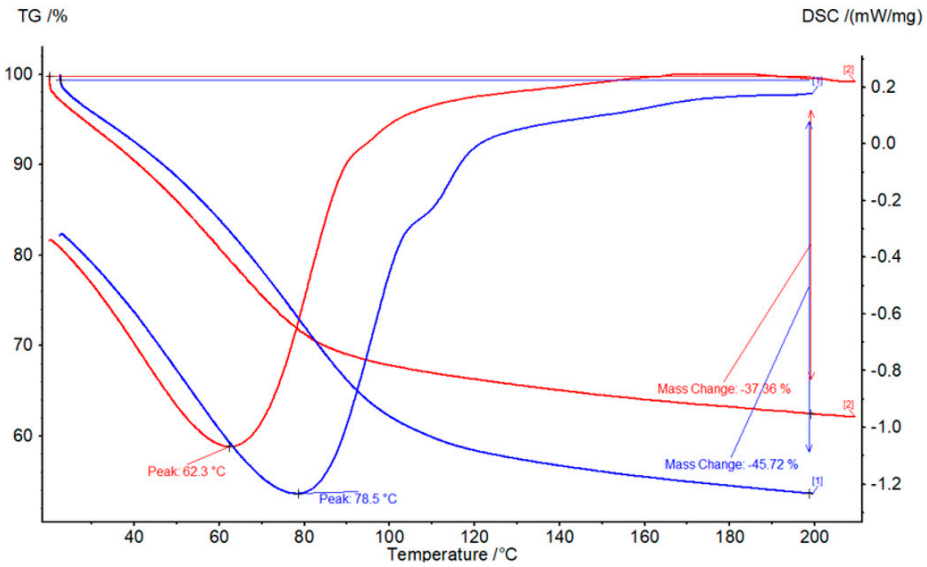

Figure 5. STA results for hydrated ENG composites with $CaCl_2$ (blue) and eutectic mixture (red) at 20 °C and 70% RH. Positive power denotes an exothermic process.

3.3. Hydration Characteristics in a Lab-Scale Reactor

The previous studies were performed in a humidity chamber and only the performance of individual composite particles was examined. This condition ensures a steady supply of humid air at a constant relative humidity, which is needed for accurate comparison between the different composites. However, to understand its performance in a real-world scenario, the particles were analyzed in a lab-scale open packed bed reactor. In this environment, the relative humidity of the feed air will decrease as it travels up the packed bed. As proven in previous hydration kinetics study (Section 3.2.2), this drop in relative humidity can impact the water uptake performance significantly, affecting instantaneous power output.

A higher system stability would mean a longer lifetime and minimized composite replacement cost. Since only ENG showed good cyclability at higher humidity, only ENG composites will be used in the next section. As composite stability has been confirmed, this section aims to understand how to maximize temperature lift and energy extraction from the particles in a packed bed reactor. Three hydration humidity levels (50%, 60%, 70%) and two flow rates (20 L/min and 30 L/min) were used at 20 °C.

3.3.1. Effect of Humidity on Cyclability

Water uptake behavior was calculated based on the absolute humidity difference between the inlet and outlet that were gathered from temperature and humidity sensors. The behavior is shown in Figure 6, and the time needed to form 6 moles of water is summarized in Table 5. As the inlet humidity and flow rate were increased, the time needed to gain 6 moles of water/mole of salt was significantly reduced. This is because an increase in humidity resulted in higher water vapor pressure while an increase in flow rate ensured high-humidity air over the whole bed, pushing the equilibrium reaction to be more product-favored and promoting water mass transport. The water uptake performance of ENG/$CaCl_2$ was better than the eutectic composite due to incomplete magnesium chloride hydrate dehydration and the less hygroscopic nature of the magnesium salt compared to calcium salt, as stated earlier. Increasing the humidity from 50% to 70% at 20 L/min reduced the time needed to uptake 6 moles of water by over 8 and 10 h for ENG/$CaCl_2$ and ENG/eutectic, respectively (Table 5). However, this is different from the results obtained in the humidity chamber, where the particles were not packed, and the humidity exposed to them was constant (Table 5). This was improved by increasing the flow rate to 30 L/min, where a 30% improvement can be seen. The difference between the two composites observed in the reactor was consistent with the results obtained from the hydration kinetics study performed in the humidity chamber (Figure 4, Section 3.2.2).

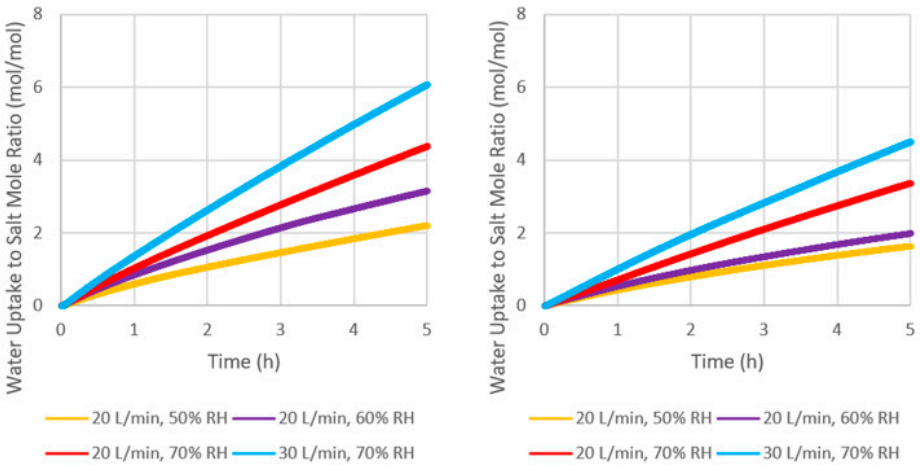

Figure 6. Mole-based water uptake behavior of (**left**) ENG/$CaCl_2$ and (**right**) ENG/eutectic.

Table 5. Time needed to uptake six moles of water by $CaCl_2$ and eutectic ENG composites in different environments at 20 °C.

	Humidity Chamber			Reactor			
Conditions	**50%**	**60%**	**70%**	**20 L/min, 50%**	**20 L/min, 60%**	**20 L/min, 70%**	**30 L/min, 70%**
ENG/$CaCl_2$	5 h	3 h	3 h	15 h	10 h	7 h	5 h
ENG/eutectic	5 h	4 h	4 h	>20 h	>20 h	10 h	7 h

3.3.2. Effect of Humidity and Flow Rate on Temperature Lift

At the beginning of hydration, the temperature lift was high due to the rapid formation of monohydrates and dihydrates (Figure 7). A lag in the time taken to achieve the highest middle and outlet temperature was observed for all experiments, usually by approximately 10 min (Figure 7). This was due to the rapid depletion of water in the air as it traveled up the column, as well as due to the sensible heating of the reactor.

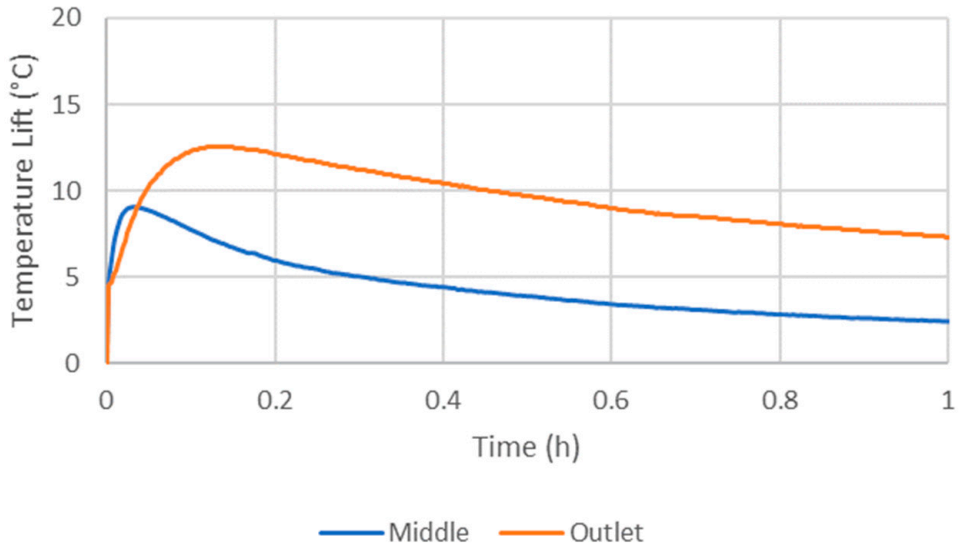

Figure 7. Example temperature lift at the middle and the outlet.

The maximum middle and outlet temperature lift for both composites are shown in Figure 8. A higher inlet humidity resulted in a greater temperature lift due to higher concentrations of water in the air. The greater the inlet humidity, the poorer ENG/eutectic performed in terms of maximum temperature lift compared to ENG/$CaCl_2$. At 50% RH, the maximum outlet temperature and water uptake were similar between ENG/$CaCl_2$ and ENG/eutectic. The highest maximum temperature lift of 16 °C was achieved using ENG/$CaCl_2$ at 20 L/min and 70% RH, which is 4 °C higher than the ENG/eutectic. In most cases, increasing the inlet flow rate decreased the maximum temperature lift despite increasing the water uptake rate. This is because the increase in the rate of water uptake did not increase by the same factor. As the flow rate was increased to 30 L/min, two composites achieved similar maximum temperature lift.

The temperature lift was observed to still be significant even after 5 h at 70% RH, obtaining over 6 °C at 20 L/min and 3 °C at 30 L/min (Figure 9).

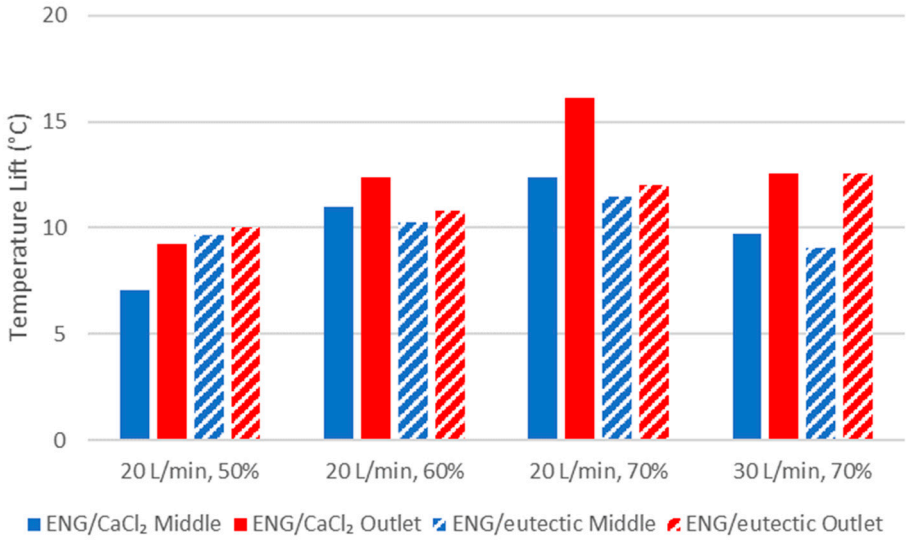

Figure 8. Comparison of maximum temperature lift achieved between $CaCl_2$ and eutectic ENG composites.

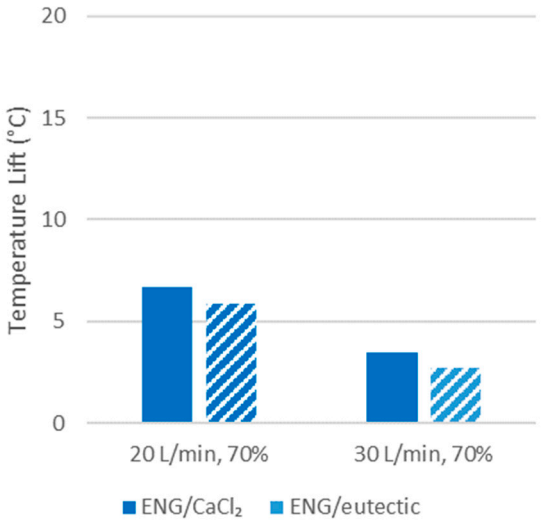

Figure 9. Temperature lift after five hours.

3.3.3. Power Output and Volumetric Thermal Energy Density

A high-power output is important for a successful TCES system. The power generation is from hydration reaction, which can be calculated via Equation (5) on composite volumetric basis (kW/m^3).

$$P_{reaction} = \frac{\Delta h_R \dot{m}_{H_2O}}{V_{matrix}} \quad (5)$$

where Δh_R is the enthalpy change of the reaction between water vapor and salt (3182 kJ/kg$_{water}$ at 25 °C [36]) and $\dot{m}_{H_2O}$ is the water uptake rate. The total generated energy is used for three areas: heat losses to ambient, sensible heating of the composites and reactor, and sensible heating of air. If the reactor is well insulated, the heat losses to ambient is negligible. If air is fed for an extended period upon completion of the reaction, then all the energy could be recovered. Hence, $P_{reaction}$ integrated over the total hydration period can also be considered the theoretical energy density.

The real power output only accounts for the sensible heating of air and is expressed as Equation (6).

$$P = \dot{V} \rho_{air} \Delta T \left(1.006 + 1.86 \left(\frac{x_{in} + x_{out}}{2} \right) \right) \quad (6)$$

where $\dot{V}$ is the volumetric air flow rate, ρ_{air} is air density, ΔT is the temperature difference between the outlet and inlet air, and x_{in} and x_{out} are the absolute humidity of the inlet and outlet air. This can also be converted to mass basis (Equation (7) and Figure 10) and volumetric basis (Equation (8) and Figure 11) for better comparison.

$$P_m = \frac{P}{m_{matrix}} \tag{7}$$

$$P_V = \frac{P}{V_{matrix}} \tag{8}$$

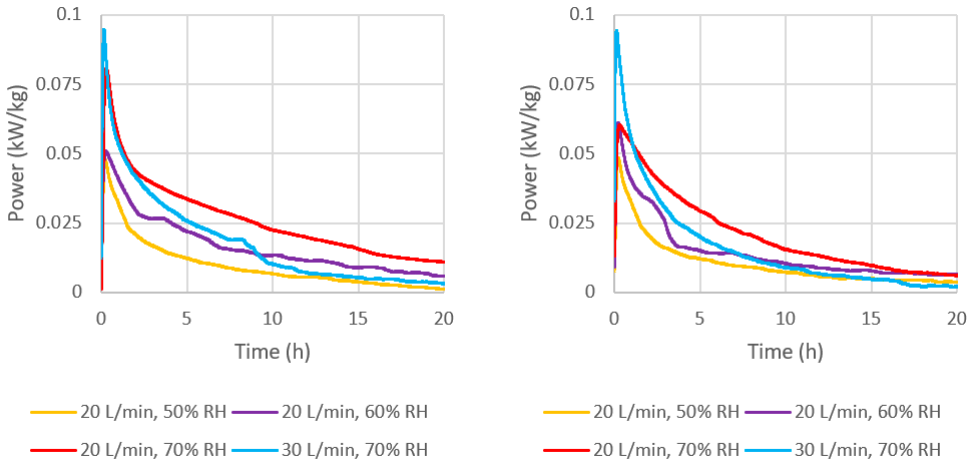

Figure 10. Mass-based reaction power output of (**left**) ENG/$CaCl_2$ and (**right**) ENG/eutectic.

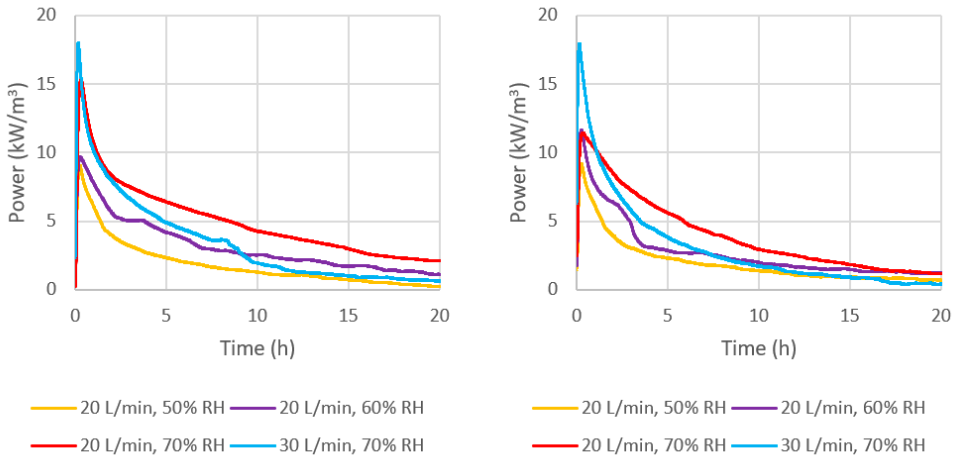

Figure 11. Volume-based reaction power output of (**left**) ENG/$CaCl_2$ and (**right**) ENG/eutectic.

It was shown in Section 3.3.2 that an increase in humidity and flow rate both increased water uptake rate (Figure 6 and Table 5), thereby also increasing the rate of heat release from the hydration reaction, resulting in higher real power output (Figures 10 and 11). It can also be observed that even though the peak power output was similar for the two composites, except for 20 L/min and 70% RH, the output from ENG/$CaCl_2$ was more persistent. This is because at lower humidity (50%), the formation rate of dihydrates was similar, but $CaCl_2$ can uptake more water than $MgCl_2$ and at a faster rate. The greater the inlet humidity, the greater the difference in power output seen between the two composites, where ENG/$CaCl_2$ performed much better. At 20 L/min and 70% RH, the $CaCl_2$ composite achieved a maximum of 0.082 kW/kg, which is higher than the eutectic composite which peaked at 0.061 kW/kg.

It is also important to evaluate the volumetric power output, where a higher value would result in smaller system volume, which is important especially given that the capital cost of reactors depends on the volume. From Figure 11, the maximum volumetric power output of ENG/$CaCl_2$ is 15.4 kW/m^3, which is 40% greater than ENG/eutectic at 20 L/min and 70% RH. As the flow rate was increased to 30 L/min at the same humidity, the highest peak power output was achieved compared to all other tested conditions, at roughly 0.094 kW/kg or 17.4 kW/m^3 by both composites; however, this leveled off much more quickly.

The volumetric thermal energy density at any time can be calculated by integration of the area under the hydration power curve (Equation (9)) from both composites at different conditions and these are shown in Figure 12. According to the results, ENG/$CaCl_2$ performed consistently better than ENG/eutectic, and the greater the inlet humidity, the greater the difference in performance. Increasing the humidity resulted in total generated power in the same amount of time; however, increasing the flow rate accomplished the opposite despite the higher power output peak. The highest energy storage achieved in 20 h was 150 kWh and 120 kWh per cubic meter of ENG/$CaCl_2$ and ENG/eutectic composites, respectively, at a low flow rate and high humidity (20 L/min and 70% RH). However, the power curve leveled off after 10 h at lower humidity (50%) due to a low reaction rate, and at a higher flow rate due to faster heat exchange. Due to the hygroscopic nature of the impregnated salt, even at 20 L/min and 50% RH, the composite can become fully hydrated after an extended time, reaching the maximum theoretical energy density in an ideal system (Table 5).

$$Q_V = \int_{t_0}^{t_1} P_V \, dt \tag{9}$$

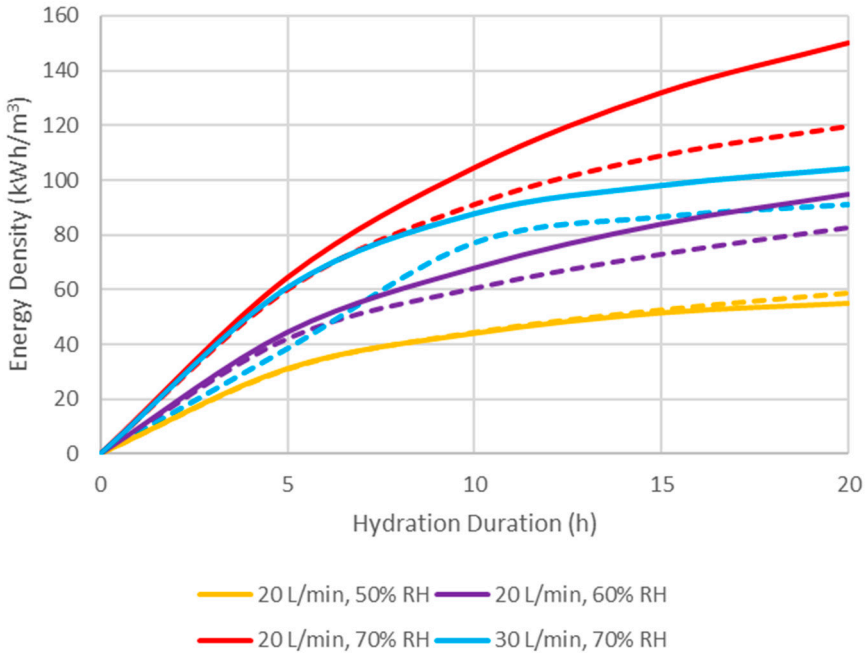

Figure 12. Achieved thermal energy density of $CaCl_2$ (solid lines) and eutectic (dotted lines) ENG composite over time under different reaction conditions.

4. Comparison, Outlook, and Future Work

For a thermochemical energy storage system to be commercially viable, the energy density must be above 150 kWh/m^3 with an implementation cost of less than USD 2–5 per kWh [37,38]. To achieve 150 kWh, the volume required for ENG/$CaCl_2$ is 0.83 m^3, while that for ENG/eutectic is 0.92 m^3, assuming sufficient optimal flow rate and inlet humidity, as well as enough reaction time to reach the theoretical energy

density. The ENG composites investigated in this study have similar or higher energy density (120 kWh/m^3 for ENG/eutectic and 150 kWh/m^3 for ENG/$CaCl_2$) compared to previous studies on Zeolite 13X (86–136 kWh/m^3 at 86–180 °C dehydration) [39–41], vermiculite/$CaCl_2$ (101–112 kWh/m^3 at 80–90 °C dehydration) [42], and cement/$SrCl_2$ (136 kWh/m^3 at 150 °C dehydration) [9] in an open packed bed reactor. Both ENG composites cost USD 3.5 per kWh for single use, which is an improvement from previous research on Zeolite 13X, cement/$SrCl_2$, and the zeolite-cement/$SrCl_2$ cascade system, at the cost of between USD 4.1/kWh and USD 8.1/kWh [9,39]. Given that the stability of ENG composites is proven up to 50 cycles for the composites, the cost per kWh for long-term use is less than USD 0.08, putting salt-in-matrix thermochemical energy storage in competition with sensible heat energy storage, which typically costs above USD 0.12/kWh [43].

It is evident that the ENG composites used in this study demonstrate excellent practical cyclability and thermal energy density. However, there are some important considerations that are beyond the scope of this work. To better understand the capabilities of ENG composites and optimize them for higher persistent power generation for practical applications, it is crucial to further investigate the mass transport resistance and reaction kinetics. As the shape of ENG is highly customizable and the composite density is not very high, fluidizing the ENG composite particles may have better results in certain applications. It is also important to evaluate the stability and cycle efficiency of multiple particles in a lab-scale reactor in the future.

5. Conclusions

ENG composites with hygroscopic salts ($CaCl_2$ and dehydrated bischofite ($MgCl_2$)) were cycled over 50 times at above deliquescence conditions to simulate challenging real-world climate conditions where the TCES might be utilized. They showed excellent stability with no leakage or mechanical deterioration over 50 cycles in the humidity chamber and 8 cycles in an open packed bed reactor, taking up to 2 g of water per gram of salt in the composite. This, along with reasonable hydration kinetics, makes expanded natural graphite composites superior to expanded clay and expanded vermiculite composites, despite having a lower theoretical energy density by 18% to 32%. A novel eutectic mixture containing 25 wt. % cheap, abundant, industry waste material, bischofite was used, lowering the composite's dehydration temperature at which the maximum mass loss rate occurred by 16.2 °C to 62.3 °C. This showed that the eutectic composite can be recharged at a lower temperature using less energy-intensive heating methods, such as solar energy or low-temperature waste heat. In addition, using the eutectic mixture lowered the composite cost by 9% from USD 627/m^3 at the cost of the same reduction in theoretical energy density. The ENG composites were applied in a lab-scale open packed bed reactor system. The maximum temperature lift and specific power output achieved were 16 °C and 0.094 kW/kg (equivalent to 17.4 kW/m^3), respectively, and between 120 and 150 kWh/m^3 of energy can be generated in 20 h. It was found that an increase in humidity and flow rate increased temperature lift, water uptake rate, and power generation. The eutectic composite performed slightly worse in all tested aspects, mainly due to the less hygroscopic nature of $MgCl_2$ and its hydrate's inability to become fully anhydrous. The initial economic analysis suggested that the ENG composites cost less than USD 0.08 per kWh per cycle, making salt-in-matrix thermochemical energy storage a strong competitor against sensible heat storage technologies, and they are feasible to be applied in a real-life system.

Author Contributions: Conceptualization, B.L. and M.F.; methodology, B.L., R.-J.C. and M.F.; formal analysis, B.L. and L.B.; investigation, B.L. and L.B.; resources, M.F. and S.U.; data curation, B.L. and L.B.; writing—original draft preparation, B.L. and L.B.; writing—review and editing, B.L., R.-J.C., S.U. and M.F.; supervision, B.L. and M.F.; project administration, M.F.; funding acquisition, M.F. All authors have read and agreed to the published version of the manuscript.

Funding: Dr. Svetlana Ushak was funded by the SERC-Chile ANID/FONDAP N° 15110019, ANID/PUENTE N° 1523A0006, and ANID/FONDECYT REGULAR Nº 1231721 projects.

Data Availability Statement: Data are contained within the article.

Acknowledgments: The authors would like to thank Raymond Hoffmann and Alec Asadov for technical assistance.

Conflicts of Interest: The authors declare no conflicts of interest.

References

1. Donkers, P.A.J.; Sögütoglu, L.C.; Huinink, H.P.; Fischer, H.R.; Adan, O.C.G. A review of salt hydrates for seasonal heat storage in domestic applications. *Appl. Energy* **2017**, *199*, 45–68. [CrossRef]
2. Kousksou, T.; Bruel, P.; Jamil, A.; El Rhafiki, T.; Zeraouli, Y. Energy storage: Applications and challenges. *Sol. Energy Mater. Sol. Cells* **2014**, *120*, 59–80. [CrossRef]
3. Cot-Gores, J.; Castell, A.; Cabeza, L.F. Thermochemical energy storage and conversion: A-state-of-the-art review of the experimental research under practical conditions. *Renew. Sustain. Energy Rev.* **2012**, *16*, 5207–5224. [CrossRef]
4. Hua, W.; Yan, H.; Zhang, X.; Xu, X.; Zhang, L.; Shi, Y. Review of salt hydrates-based thermochemical adsorption thermal storage technologies. *J. Energy Storage* **2022**, *56*, 106158. [CrossRef]
5. Fischer, M.; Bruzzano, S.; Egenolf-Jonkmanns, B.; Zeidler-Fandrich, B.; Wack, H.; Deerberg, G. Thermal Storage by Thermoreversible Chemical Reaction Systems. *Energy Procedia* **2014**, *48*, 327–336. [CrossRef]
6. Druske, M.-M.; Fopah-Lele, A.; Korhammer, K.; Rammelberg, H.U.; Wegscheider, N.; Ruck, W.; Schmidt, T. Developed Materials for Thermal Energy Storage: Synthesis and Characterization. *Energy Procedia* **2014**, *61*, 96–99. [CrossRef]
7. Mehrabadi, A.; Farid, M. New salt hydrate composite for low-grade thermal energy storage. *Energy* **2018**, *164*, 194–203. [CrossRef]
8. Michel, B.; Mazet, N.; Mauran, S.; Stitou, D.; Xu, J. Thermochemical process for seasonal storage of solar energy: Characterization and modeling of a high density reactive bed. *Energy* **2012**, *47*, 553–563. [CrossRef]
9. Clark, R.-J.; Farid, M. Experimental investigation into the performance of novel $SrCl_2$-based composite material for thermochemical energy storage. *J. Energy Storage* **2021**, *36*, 102390. [CrossRef]
10. Lahmidi, H.; Mauran, S.; Goetz, V. Definition, test and simulation of a thermochemical storage process adapted to solar thermal systems. *Sol. Energy* **2006**, *80*, 883–893. [CrossRef]
11. Mauran, S.; Lahmidi, H.; Goetz, V. Solar heating and cooling by a thermochemical process. First experiments of a prototype storing 60kWh by a solid/gas reaction. *Sol. Energy* **2008**, *82*, 623–636. [CrossRef]
12. Zhao, Y.J.; Wang, R.Z.; Zhang, Y.N.; Yu, N. Development of $SrBr_2$ composite sorbents for a sorption thermal energy storage system to store low-temperature heat. *Energy* **2016**, *115*, 129–139. [CrossRef]
13. Ousaleh, H.A.; Sair, S.; Mansouri, S.; Abboud, Y.; Faik, A.; El Bouari, A. New hybrid graphene/inorganic salt composites for thermochemical energy storage: Synthesis, cyclability investigation and heat exchanger metal corrosion protection performance. *Sol. Energy Mater. Sol. Cells* **2020**, *215*, 110601. [CrossRef]
14. Opel, O.; Rammelberg, H.U.; Gérard, M.; Ruck, W. Thermochemical storage materials research-TGA/DSC-hydration studies. In Proceedings of the International Conference for Sustainable Energy Storage, Belfast, UK, 21–24 February 2011.
15. Korhammer, K.; Druske, M.-M.; Fopah-Lele, A.; Rammelberg, H.U.; Wegscheider, N.; Opel, O.; Osterland, T.; Ruck, W. Sorption and thermal characterization of composite materials based on chlorides for thermal energy storage. *Appl. Energy* **2016**, *162*, 1462–1472. [CrossRef]
16. Gaeini, M.; Rouws, A.L.; Salari, J.W.O.; Zondag, H.A.; Rindt, C.C.M. Characterization of microencapsulated and impregnated porous host materials based on calcium chloride for thermochemical energy storage. *Appl. Energy* **2018**, *212*, 1165–1177. [CrossRef]
17. Ousaleh, H.A.; Sair, S.; Zaki, A.; Younes, A.; Faik, A.; El Bouari, A. Advanced experimental investigation of double hydrated salts and their composite for improved cycling stability and metal compatibility for long-term heat storage technologies. *Renew. Energy* **2020**, *162*, 447–457. [CrossRef]
18. Miao, Q.; Zhang, Y.; Jia, X.; Li, Z.; Tan, L.; Ding, Y. $MgSO_4$-expanded graphite composites for mass and heat transfer enhancement of thermochemical energy storage. *Sol. Energy* **2021**, *220*, 432–439. [CrossRef]
19. Li, W.; Klemeš, J.J.; Wang, Q.; Zeng, M. Development and characteristics analysis of salt-hydrate based composite sorbent for low-grade thermochemical energy storage. *Renew. Energy* **2020**, *157*, 920–940. [CrossRef]
20. Li, W.; Klemeš, J.J.; Wang, Q.; Zeng, M. Characterisation and sorption behaviour of LiOH-LiCl@EG composite sorbents for thermochemical energy storage with controllable thermal upgradeability. *Chem. Eng. J.* **2021**, *421*, 129586. [CrossRef]
21. Zhao, Q.; Lin, J.; Huang, H.; Xie, Z.; Xiao, Y. Enhancement of heat and mass transfer of potassium carbonate-based thermochemical materials for thermal energy storage. *J. Energy Storage* **2022**, *50*, 104259. [CrossRef]
22. Fisher, R.; Ding, Y.; Sciacovelli, A. Hydration kinetics of K_2CO_3, $MgCl_2$ and vermiculite-based composites in view of low-temperature thermochemical energy storage. *J. Energy Storage* **2021**, *38*, 102561. [CrossRef]
23. Salviati, S.; Carosio, F.; Cantamessa, F.; Medina, L.; Berglund, L.A.; Saracco, G.; Fina, A. Ice-templated nanocellulose porous structure enhances thermochemical storage kinetics in hydrated salt/graphite composites. *Renew. Energy* **2020**, *160*, 698–706. [CrossRef]
24. Zhang, Y.N.; Wang, R.Z.; Zhao, Y.J.; Li, T.X.; Riffat, S.B.; Wajid, N.M. Development and thermochemical characterizations of vermiculite/$SrBr_2$ composite sorbents for low-temperature heat storage. *Energy* **2016**, *115*, 120–128. [CrossRef]

25. Sutton, R.J.; Jewell, E.; Elvins, J.; Searle, J.R.; Jones, P. Characterising the discharge cycle of $CaCl_2$ and $LiNO_3$ hydrated salts within a vermiculite composite scaffold for thermochemical storage. *Energy Build.* **2018**, *162*, 109–120. [CrossRef]
26. Nejhad, M.K.; Aydin, D. Synthesize and hygro-thermal performance analysis of novel APC-$CaCl_2$ composite sorbent for low-grade heat recovery, storage, and utilization. *Energy Sources Part A Recovery Util. Environ. Eff.* **2019**, *43*, 3011–3031. [CrossRef]
27. Aristov, Y.I.; Restuccia, G.; Tokarev, M.M.; Cacciola, G. Selective Water Sorbents for Multiple Applications. *React. Kinet. Catal. Lett.* **2000**, *69*, 345–353. [CrossRef]
28. N'Tsoukpoe, K.E.; Schmidt, T.; Rammelberg, H.U.; Watts, B.A.; Ruck, W.K.L. A systematic multi-step screening of numerous salt hydrates for low temperature thermochemical energy storage. *Appl. Energy* **2014**, *124*, 1–16. [CrossRef]
29. Ushak, S.; Gutierrez, A.; Galleguillos, H.; Fernandez, A.G.; Cabeza, L.F.; Grágeda, M. Thermophysical characterization of a by-product from the non-metallic industry as inorganic PCM. *Sol. Energy Mater. Sol. Cells* **2015**, *132*, 385–391. [CrossRef]
30. Li, P.; Liu, B.; Lai, X.; Liu, W.; Gao, L.; Tang, Z. Thermal decomposition mechanism and pyrolysis products of waste bischofite calcined at high temperature. *Thermochim. Acta* **2022**, *710*, 179164. [CrossRef]
31. El-Sebaii, A.A.; Al-Amir, S.; Al-Marzouki, F.M.; Faidah, A.S.; Al-Ghamdi, A.A.; Al-Heniti, S. Fast thermal cycling of acetanilide and magnesium chloride hexahydrate for indoor solar cooking. *Energy Convers. Manag.* **2009**, *50*, 3104–3111. [CrossRef]
32. Li, G.; Zhang, B.; Li, X.; Zhou, Y.; Sun, Q.; Yun, Q. The preparation, characterization and modification of a new phase change material: $CaCl_2{\cdot}6H_2O$–$MgCl_2{\cdot}6H_2O$ eutectic hydrate salt. *Sol. Energy Mater. Sol. Cells* **2014**, *126*, 51–55. [CrossRef]
33. Ye, Z.; Liu, H.; Wang, W.; Liu, H.; Lv, J.; Yang, F. Reaction/sorption kinetics of salt hydrates for thermal energy storage. *J. Energy Storage* **2022**, *56*, 106122. [CrossRef]
34. Kosny, J.; Shukla, N.; Fallahi, A. *Cost Analysis of Simple Phase Change Material—Enhanced Building Envelopes in Southern US Climates*; National Renewable Energy Laboratory (NREL): Golden, CO, USA, 2013.
35. Molenda, M.; Stengler, J.; Linder, M.; Wörner, A. Reversible hydration behavior of $CaCl_2$ at high H_2O partial pressures for thermochemical energy storage. *Thermochim. Acta* **2013**, *560*, 76–81. [CrossRef]
36. Rambaud, G.; Mauran, S.; Mazet, N. Problématique des Transferts en Milieu Poreux Réactif Déformable Pour Procédés de Rafraîchissement Solaire. Ph.D. Thesis, Université de Perpignan, Perpignan, France, 2009.
37. Courbon, E.; D'Ans, P.; Permyakova, A.; Skrylnyk, O.; Steunou, N.; Degrez, M.; Frère, M. A new composite sorbent based on $SrBr_2$ and silica gel for solar energy storage application with high energy storage density and stability. *Appl. Energy* **2017**, *190*, 1184–1194. [CrossRef]
38. Rommel, M.; Hauer, A.; van Helden, W. IEA SHC Task 42/ECES Annex 29 Compact Thermal Energy Storage. *Energy Procedia* **2016**, *91*, 226–230. [CrossRef]
39. Clark, R.-J.; Farid, M. Experimental investigation into cascade thermochemical energy storage system using $SrCl_2$-cement and zeolite-13X materials. *Appl. Energy* **2022**, *316*, 119145. [CrossRef]
40. Han, X.; Liu, S.; Zeng, C.; Yang, L.; Shukla, A.; Shen, Y. Investigating the performance enhancement of copper fins on trapezoidal thermochemical reactor. *Renew. Energy* **2020**, *150*, 1037–1046. [CrossRef]
41. van Alebeek, R.; Scapino, L.; Beving, M.A.J.M.; Gaeini, M.; Rindt, C.C.M.; Zondag, H.A. Investigation of a household-scale open sorption energy storage system based on the zeolite 13X/water reacting pair. *Appl. Therm. Eng.* **2018**, *139*, 325–333. [CrossRef]
42. Aydin, D.; Casey, S.P.; Chen, X.; Riffat, S. Novel "open-sorption pipe" reactor for solar thermal energy storage. *Energy Convers. Manag.* **2016**, *121*, 321–334. [CrossRef]
43. Sarbu, I.; Sebarchievici, C. A Comprehensive Review of Thermal Energy Storage. *Sustainability* **2018**, *10*, 191. [CrossRef]